Research article JHEP|Reports

Steatosis drives monocyte-derived macrophage accumulation in human metabolic dysfunction-associated fatty liver disease

Authors

Mandy M. Chan, Sabine Daemen, Joseph W. Beals, Marina Terekhova, Bin Q. Yang, Christina F. Fu, Li He, Arick C. Park, Gordon I. Smith, Babak Razani, Kathleen Byrnes, Wandy L. Beatty, Shaina R. Eckhouse, J. Christopher Eagon, Daniel Ferguson, Brian N. Finck, Samuel Klein, Maxim N. Artyomov, Joel D. Schilling

Correspondence

schillij@wustl.edu (J.D. Schilling).

Graphical abstract

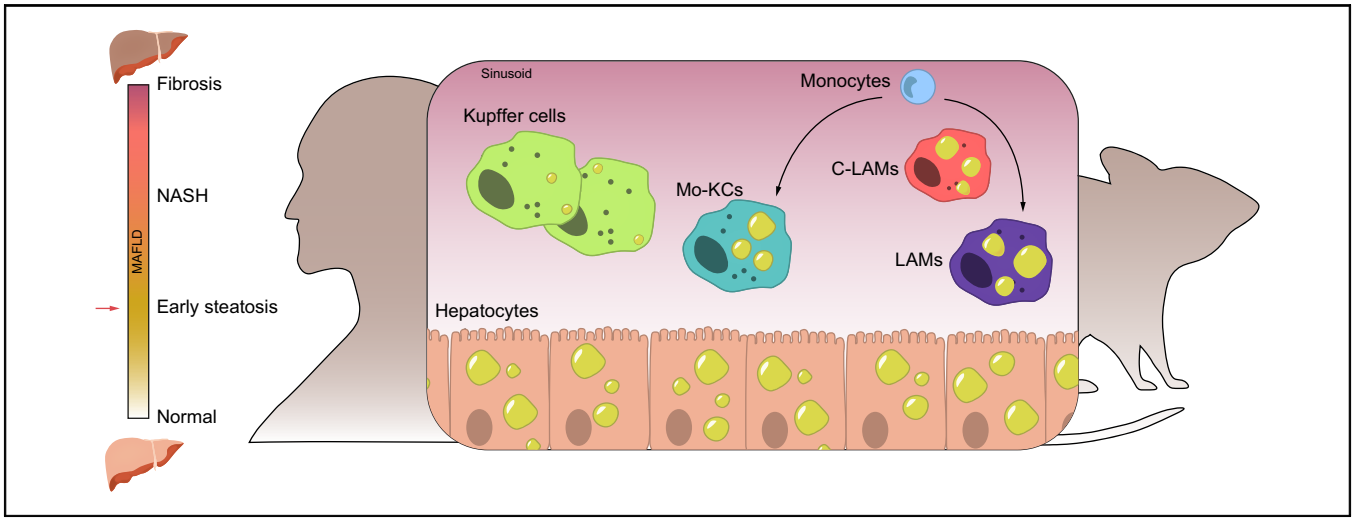

Highlights

- In early MAFLD, the human liver contains diverse macrophage subsets.
- Macrophage subtypes present in MAFLD align between humans and mice.
- Monocyte-derived macrophages increase in the liver with steatosis.
- Kupffer cell loss is not required for monocyte recruitment.
- Recruited macrophages can take up fatty acids released by steatotic hepatocytes.

Impact and implications

Metabolic dysfunction associated fatty liver disease (MAFLD) is extremely common; however, the early inflammatory responses that occur in human disease are not well understood. In this study, we investigated macrophage heterogeneity in human livers during early MAFLD and demonstrated that similar shifts in macrophage subsets occur in human disease that are similar to those seen in preclinical models. These findings are important as they establish a translational link between mouse and human models of disease, which is important for the development and testing of new therapeutic approaches for MAFLD.

https://doi.org/10.1016/j.jhepr.2023.100877

Research article

JHEP|Reports

Steatosis drives monocyte-derived macrophage accumulation in human metabolic dysfunction-associated fatty liver disease

Mandy M. Chan,[1,2,3] Sabine Daemen,[4] Joseph W. Beals,[5] Marina Terekhova,[3] Bin Q. Yang,[6] Christina F. Fu,[1,2,3] Li He,[1,2] Arick C. Park,[2] Gordon I. Smith,[5] Babak Razani,[7,8] Kathleen Byrnes,[3] Wandy L. Beatty,[9] Shaina R. Eckhouse,[10] J. Christopher Eagon,[10] Daniel Ferguson,[5] Brian N. Finck,[5] Samuel Klein,[5] Maxim N. Artyomov,[3] Joel D. Schilling[1,2,3,*]

[1]*Diabetes Research Center, Washington University School of Medicine, St. Louis, MO, USA;* [2]*Department of Medicine, Washington University School of Medicine, St. Louis, MO, USA;* [3]*Department of Pathology and Immunology, Washington University School of Medicine, St. Louis, MO, USA;* [4]*Department of Internal Medicine, Cardiovascular Research Institute Maastricht, Maastricht University Medical Center, Maastricht, The Netherlands;* [5]*Center for Human Nutrition, Washington University School of Medicine, St. Louis, MO, USA;* [6]*Division of Cardiology, Massachusetts General Hospital, Harvard Medical School, Boston, MA, USA;* [7]*Vascular Medicine Institute, Department of Medicine, University of Pittsburgh School of Medicine and UPMC, Pittsburgh, PA, USA;* [8]*Division of Cardiology, Pittsburgh VA Medical Center, Pittsburgh, PA, USA;* [9]*Department of Molecular Microbiology, Washington University School of Medicine, St. Louis, MO, USA;* [10]*Department of Surgery, Washington University School of Medicine, St. Louis, MO, USA*

JHEP Reports **2023.** https://doi.org/10.1016/j.jhepr.2023.100877

Background & Aims: Metabolic dysfunction-associated fatty liver disease (MAFLD) is a common complication of obesity with a hallmark feature of hepatic steatosis. Recent data from animal models of MAFLD have demonstrated substantial changes in macrophage composition in the fatty liver. In humans, the relationship between liver macrophage heterogeneity and liver steatosis is less clear.

Methods: Liver tissue from 21 participants was collected at time of bariatric surgery and analysed using flow cytometry, immunofluorescence, and H&E microscopy. Single-cell RNA sequencing was also conducted on a subset of samples (n = 3). Intrahepatic triglyceride content was assessed via MRI and tissue histology. Mouse models of hepatic steatosis were used to investigate observations made from human liver tissue.

Results: We observed variable degrees of liver steatosis with minimal fibrosis in our participants. Single-cell RNA sequencing revealed four macrophage clusters that exist in the human fatty liver encompassing Kupffer cells and monocyte-derived macrophages (MdMs). The genes expressed in these macrophage subsets were similar to those observed in mouse models of MAFLD. Hepatic $CD14^+$ monocyte/macrophage number correlated with the degree of steatosis. Using mouse models of early liver steatosis, we demonstrate that recruitment of MdMs precedes Kupffer cell loss and liver damage. Electron microscopy of isolated macrophages revealed increased lipid accumulation in MdMs, and *ex vivo* lipid transfer experiments suggested that MdMs may serve a distinct role in lipid uptake during MAFLD.

Conclusions: The human liver in MAFLD contains macrophage subsets that align well with those that appear in mouse models of fatty liver disease. Recruited myeloid cells correlate well with the degree of liver steatosis in humans. MdMs appear to participate in lipid uptake during early stages of MALFD.

Impact and implications: Metabolic dysfunction associated fatty liver disease (MAFLD) is extremely common; however, the early inflammatory responses that occur in human disease are not well understood. In this study, we investigated macrophage heterogeneity in human livers during early MAFLD and demonstrated that similar shifts in macrophage subsets occur in human disease that are similar to those seen in preclinical models. These findings are important as they establish a translational link between mouse and human models of disease, which is important for the development and testing of new therapeutic approaches for MAFLD.

Introduction

Non-alcoholic fatty liver disease (NAFLD), now often referred to as metabolic dysfunction-associated fatty liver disease (MAFLD), is a leading cause of liver failure in the world.[1] MAFLD develops in the context of obesity and/or diabetes and can progress to an inflammatory liver condition known as non-alcoholic steatohepatitis (NASH).[2] NASH is associated with an increased risk of cirrhosis and hepatocellular carcinoma and is quickly becoming the predominant condition requiring liver transplantation.[3,4] However, the factors that dictate the progression of simple steatosis to NASH are not well understood.

Keywords: Obesity; Kupffer cells; Inflammation; Liver steatosis.
Received 23 January 2023; received in revised form 28 July 2023; accepted 3 August 2023; available online 11 August 2023

* Corresponding author. Address: Diabetes Research Center, Division of Cardiology, Washington University School of Medicine, St. Louis, MO 63110, USA. Tel.:314-747-8499; Fax: 314-747-0264
E-mail address: schillij@wustl.edu (J.D. Schilling).

Mouse models of MAFLD and NASH produce many of the hallmarks of the human disease including liver steatosis, hepatocyte injury, inflammation, hepatocellular carcinoma, and fibrosis. Recent studies using fate mapping, single-cell RNA sequencing (scRNA-seq), multicolour flow cytometry, and tissue imaging have elucidated a shift in macrophage composition that occurs with the progression of fatty liver disease.[5–8] Specifically, resident macrophages termed Kupffer cells (KCs) decrease in number, whereas new subsets of monocyte-derived macrophages (MdMs) enter the liver. Based on gene expression and surface markers, these MdMs can be subdivided into monocyte-derived KCs (Mo-KCs), which share many transcriptional signatures of KCs and are thought to replace lost resident cells, and hepatic lipid-associated macrophages (LAMs), which express genes characteristic of macrophages from obese adipose tissue such as *Trem2*, *Cd9*, and *Gpnmb*.[9] A subset of LAMs also express *Ccr2*/*Cx3cr1*, and these macrophages have been referred to as C-LAMs.[5,10,11] LAMs accumulate in regions of lipid accumulation and fibrosis and appear to regulate tissue remodelling.[5,12] These observations suggest that macrophages may be a therapeutic target in MAFLD.

Liver macrophage biology in human MAFLD is less well understood. This is largely attributable to the challenges in acquiring adequate samples of human liver tissue from patients at early *vs.* late stages of the disease. Moreover, it is difficult to perform multiple orthogonal assays with the amount of liver tissue obtained via transjugular or percutaneous approaches. Over the past few years, scRNA-seq, spatial proteomics, and imaging have been used to explore immune cell heterogeneity in the human liver.[13–16] Based on these studies, resident KCs have been shown to have a gene and protein expression signature that is conserved across several species. However, the changes that occur in macrophage subsets with MAFLD are less clear and more conflicting.[13,15] Thus, the agreement between human and mouse liver macrophage compositional and phenotypic changes with MAFLD progression remains controversial.

The aim of this study was to evaluate the relationship between liver macrophage phenotype and tissue pathology in participants undergoing bariatric surgery for the treatment of morbid obesity. We obtained liver wedge biopsies during bariatric surgery to conduct multiple analyses including tissue imaging, flow cytometry, and scRNA-seq. Herein, we describe the relationship between steatosis and liver monocyte/macrophage populations in humans and compare our findings with those of mouse models of MAFLD.

Materials and methods

Patients and sample collection

Twenty-six women with obesity (age 47 ± 6 years; BMI 48 ± 8 kg/m^2) scheduled for bariatric surgery were recruited to participate in the study. Participants provided written, informed consent before participating in these studies, and the study protocol conformed to the ethical guidelines of the Declaration of Helsinki and was approved by the Human Research Protection Office at Washington University School of Medicine in St. Louis, MO. Participants were part of an ongoing study investigating the effect of weight loss on liver health and metabolic function registered at ClinicalTrials.gov (NCT03701828). Results presented here are limited to only baseline samples owing to the small liver sample size collected post weight loss, which was insufficient to perform flow cytometry or scRNA-seq analyses. Participants were recruited through the Bariatric Surgery Clinic at Barnes-Jewish Hospital. Study visits were conducted in the Clinical Translational Research Unit, the Center for Clinical Imaging Research at Washington University School of Medicine, and Barnes-Jewish Hospital in St. Louis, MO. All participants completed a comprehensive screening evaluation that included a medical history and physical examination, standard blood tests, and a haemoglobin A_{1c} ($HgbA_{1c}$) test to determine eligibility. Exclusion criteria consisted of the following: (1) regular use of tobacco products; (2) excessive consumption of alcohol (≥three drinks/day for men and ≥two drinks/day for women); (3) previous intestinal resection; (4) use of any medication that can affect hepatic metabolic function; (5) evidence of coagulation problems; (6) pregnant or breastfeeding; (7) metal implants that preclude magnetic resonance testing; (8) liver disease other than MAFLD (*e.g.* hepatitis); (9) cancer diagnosis within the previous 5 years; and (10) serious chronic disease (*e.g.* kidney failure).

Mouse colony and mouse model of MAFLD

Six-week-old C57BL/6 female mice were purchased from Jackson Laboratory and acclimated to Washington University in St. Louis animal facilities for 2 weeks. At 8 weeks old, these mice were placed on either high-fat, high-sucrose, and high-cholesterol (HFSC) diet (42% kcal/fat diet with increased sucrose and 1.25% cholesterol; Teklad-TD.120528; ENVIGO, Indianapolis, IN, USA) for 8 weeks or a standard chow diet (STD) also for 8 weeks. Another cage of female mice, now at 14 weeks old, was initiated on a choline-deficient amino acid (CDAA) diet (L-amino acid diet with 45 kcal% fat with 0.1% methionine and no added choline; Research Diets A06071309, New Brunswick, NJ, USA) for 2 weeks such that all the animals are sacrificed at the same time. The weight of the animals was monitored and recorded every 2 weeks. Another set of 8-week-old C57BL/6 male mice from Jackson Laboratory was placed on HFSC diet for 16 weeks and used to obtain liver macrophages for transmission electron microscopy. All the animals were euthanised by carbon dioxide at the conclusion of the diet study. All mouse studies were approved by the Washington University in St. Louis Institutional Animal Care and Use Committee.

Please see Supplementary information for detailed methods.

Results

Collection and analysis of liver tissue from patients with MAFLD

A total of 26 participants were enrolled in the study. However, there were five patients who did not have complete flow cytometry analysis conducted on liver samples, two patients lacking magnetic resonance imaging (MRI) data, and four patients for whom tissue fibrosis imaging and/or H&E tissue sections were not available. Therefore, we had a total of 21 participants with complete data for analysis (Fig. 1A). Participants were an entirely female cohort with morbid obesity (Fig. 1B). The prevalence of diabetes was 29%, but the majority were well controlled with an average $HgbA_{1c}$ of 5.8%. Other patient characteristics are shown in Fig. 1B and Table S1. An average of 1.3 g (range 0.15–2.9 g) of tissue was collected per patient. The fresh tissue was washed and then processed for flow cytometry and imaging (frozen/deparaffinised sections for immunofluorescence and paraffinised tissue for histology and scoring; Fig. 1). In addition, three randomly chosen samples underwent flow sorting for $CD45^+$ cells followed by scRNA-seq analysis.

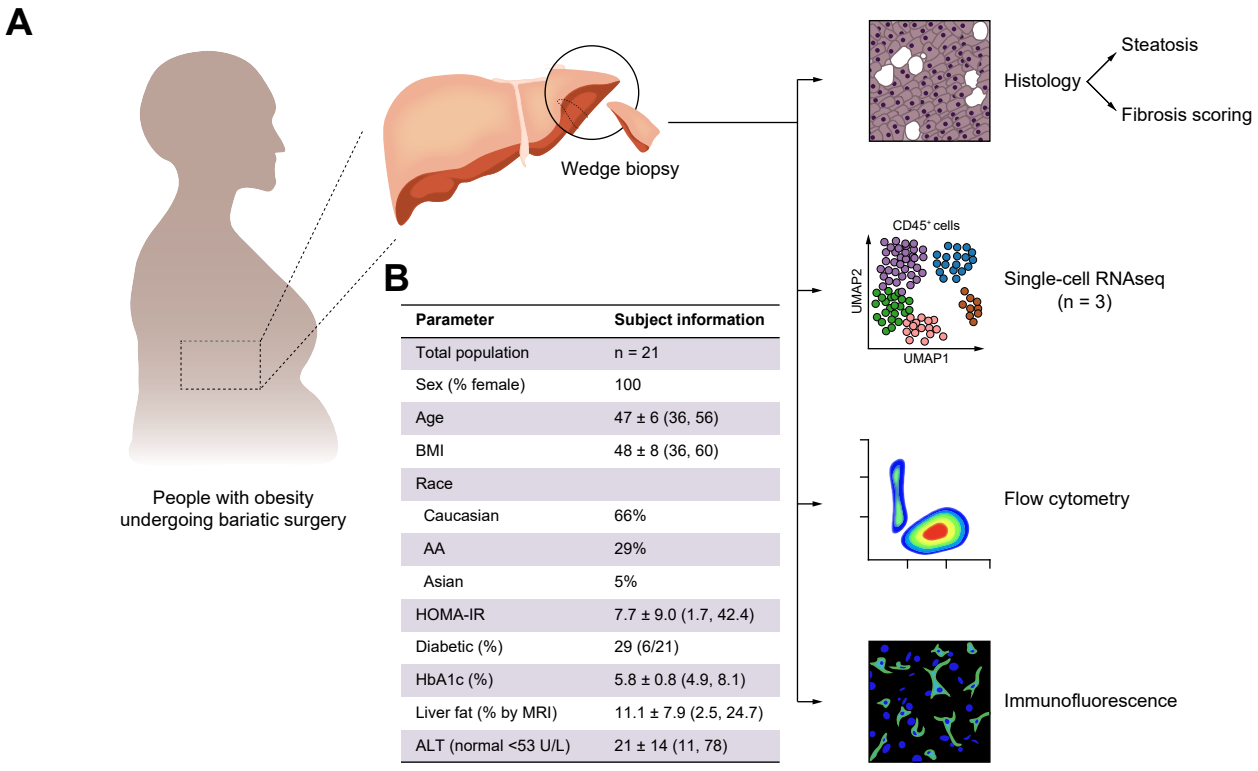

B

Parameter	Subject information
Total population	n = 21
Sex (% female)	100
Age	47 ± 6 (36, 56)
BMI	48 ± 8 (36, 60)
Race	
Caucasian	66%
AA	29%
Asian	5%
HOMA-IR	7.7 ± 9.0 (1.7, 42.4)
Diabetic (%)	29 (6/21)
HbA1c (%)	5.8 ± 0.8 (4.9, 8.1)
Liver fat (% by MRI)	11.1 ± 7.9 (2.5, 24.7)
ALT (normal <53 U/L)	21 ± 14 (11, 78)

Fig. 1. Tissue pipeline for liver analysis in patients with MAFLD. (A) Schematic of tissue harvest and analytic processes for human liver samples. (B) Table of patient demographics. AA, African American; ALT, alanine aminotransferase; $HgbA_{1c}$, haemoglobin A_{1c}; HOMA-IR, homoeostatic model assessment for insulin resistance; MAFLD, metabolic dysfunction-associated fatty liver disease; MRI, magnetic resonance imaging; RNA-seq, RNA sequencing; UMAP, uniform manifold approximation and projection.

Spectrum of liver steatosis and fibrosis in this patient cohort

On average, liver fat by MRI was ∼ 11% with a range of 2.5 to 24.7% (grade 0 to grade 1 steatosis). Approximately half of the patients had no or mild steatosis (≤5%), whereas the remainder were equally divided between moderate (6–14%) and high (≥15%) degrees of steatosis (Fig. 2A). In addition to MRI assessment, H&E-stained slides from the wedge biopsy samples were scored for percent steatosis by a pathologist blinded to the MRI results. On average, liver fat by tissue pathology was 9.5% with a range of 0 to 40% and a similar distribution compared with MRI (Fig. 2B and D). Given the potential for sampling error with the harvested liver tissue, we compared tissue steatosis quantified by intrahepatic triglyceride of the whole liver by MRI with pathologic assessment of tissue samples and found an excellent correlation (Fig. 2C). These findings highlight two important points: (1) the spectrum of steatosis represented by this patient cohort could be leveraged to evaluate the association of immunologic data with the extent of liver fat and (2) liver biopsy sections aligned well with whole tissue imaging, suggesting that data obtained from analysis of the liver biopsy tissue would likely be representative.

Liver fibrosis scoring was conducted by the same blinded pathologist using Picrosirius Red-stained sections. The majority of patients had either no fibrosis or stage 1 fibrosis (Fig. 2E and F). The degree of fibrosis was not associated with the degree of steatosis; however, those with higher fibrosis grades tended to have less steatosis (Fig. 2G). We also used the NAFLD activity score (NAS), which is a validated method to assess the presence of NASH using multiple histologic features of NASH (steatosis, lobular inflammation, and ballooning).[17] The distribution of NAS and lobular inflammation scores for our cohort is shown in Fig. 2H and I. A NAS score of 5 or greater is indicative of overt NASH, and there were two participants in our cohort who reached this threshold. Thus, the participants in this study represent an earlier stage of MAFLD pathology with variable degrees of steatosis, mild fibrosis, and rare NASH. Consistent with this, only one participant had an alanine aminotransferase level above the normal range (>53 U/L; Fig. 1B).

Heterogeneity of human macrophages and monocytes

To gain insight into the populations of myeloid cells that exist within the human fatty liver, we conducted scRNA-seq on $CD45^+$ cells isolated from three patients. Owing to the scheduling workflow and need for live cells, the liver samples chosen for scRNA-seq had to be determined ahead of time. Therefore, we chose three consecutive participants and pooled the individual data from each of these participants together for analysis. The participants used for scRNA-seq included one with moderate steatosis (10%) and two with high steatosis (∼25%). The baseline characteristics of these participants are shown in Table S2. Although all $CD45^+$ cells were analysed for these three participants (Fig. S1A), we focused on the recovered myeloid subsets. The cell recovery, gene count, and unique molecular identifier data are included in Tables S3 and S4. The myeloid cell zoom (2,985 cells) revealed eight distinct clusters using linage-defining markers that included two subsets of monocytes (*CD14*^{hi} and *CD16*^{hi}), three subsets of dendritic cells (DCs; namely, conventional DC 1 [cDC1], conventional DC 2 [cDC2], and plasmacytoid DC), two clusters of macrophages (KC and MdM), and proliferating cells (Fig. 3A). To compensate for the lack of healthy control

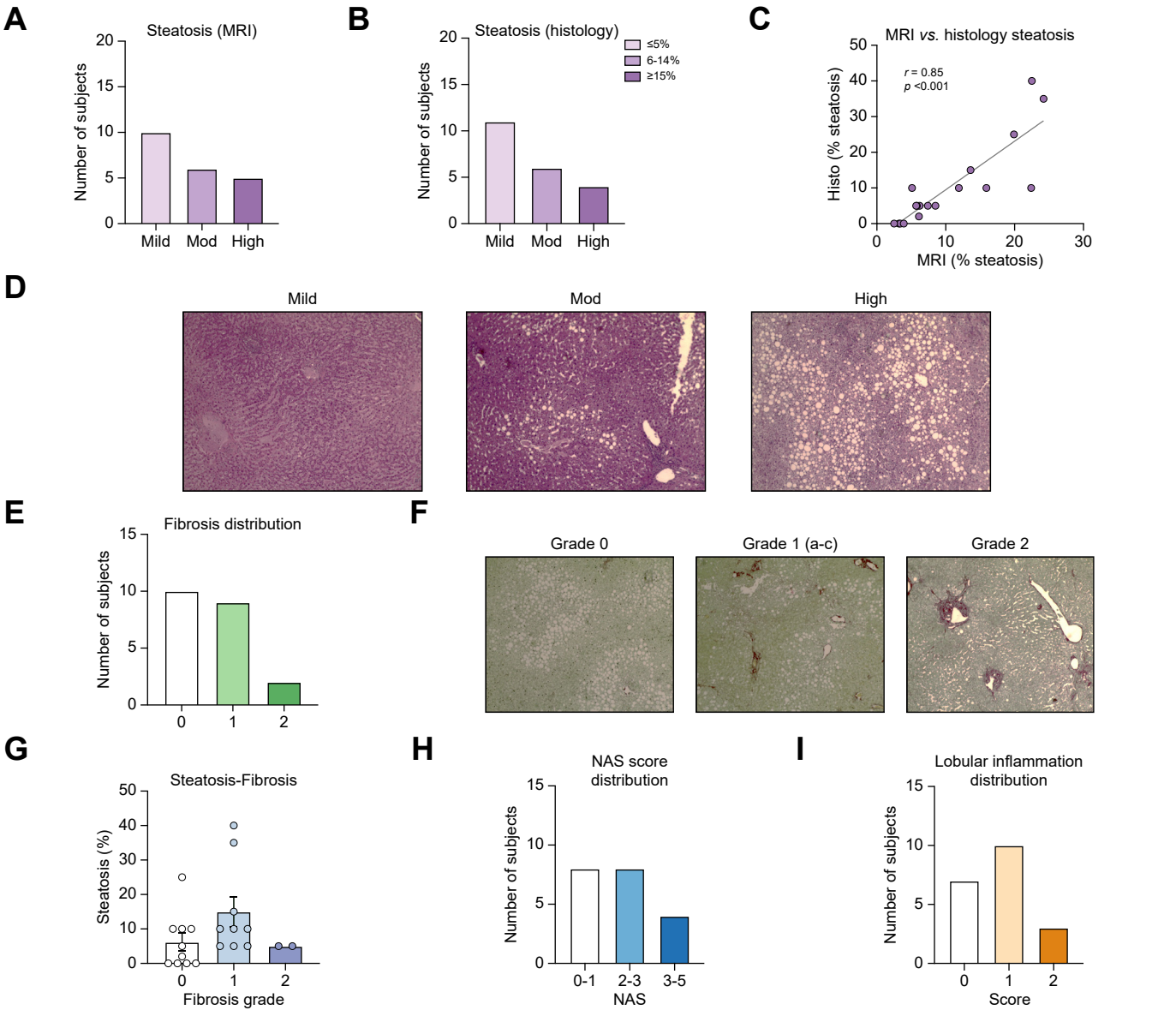

Fig. 2. Characterisation of liver steatosis and fibrosis. (A, B) Distribution of steatosis among the 21 participants in the study as quantified by (A) MRI or (B) histology. (C) Correlational analysis of steatosis quantification between MRI and histological assessment. Value of *p* is shown (Pearson correlation coefficient). (D) Representative H&E images of liver steatosis from each of the graded groups. (E) Distribution of fibrosis grades across the patient cohort. (F) Representative images from patients with the indicated classification score. (G) Association of histologic steatosis (%) with tissue fibrosis scoring. (H) Distribution of NAS score across the cohort. (I) Lobular inflammation score distribution in the enrolled patients. mod, moderate; MRI, magnetic resonance imaging; NAFLD, non-alcoholic fatty liver disease; NAS, NAFLD activity score.

livers in our study, we also integrated our data with two other recent studies from Andrews *et al.*[18] and Guilliams *et al.*[13] that included scRNA-seq data on liver myeloid populations on relatively healthy participants (Fig. 3A and B). All of the myeloid clusters identified were present in each of the individual patient samples across the three studies (Fig. S1B and C). Analysis of myeloid cell composition across studies did not reveal large shifts in cell populations although cDC2s and the MdMs tended to be higher in our steatotic samples (Fig. 3B). Heatmap analysis of the top four expressed genes in each of the cell clusters demonstrated the separation in core genes across the clusters (Fig. 3D). The top 15 genes defining each cluster are shown in Table S5. As can be appreciated in the violin plots, *CD163* was most robustly expressed in KCs, whereas *CD9* was most highly expressed in the MdMs (Fig. 3E). In addition, monocyte subsets had higher expression of *S100A8* and lower expression of MHC class II (MHCII) compared with the other myeloid cells (Fig. 3E). Additional gene expression data across monocyte and macrophage subsets are shown in Fig. S2.

It is now appreciated that several distinct macrophage subpopulations appear in the liver during the progression of fatty liver disease. However, much of the data regarding macrophage diversity in MAFLD has come from mouse models of the disease.[19] To assess macrophage phenotypes in human MAFLD, we further subclustered the macrophage clusters (959 cells) and identified four populations of macrophages (Fig. 4A). The largest cluster was that of KCs, which were marked by high expression of *CD163*, *MARCO*, and *TIMD4* (Fig. 4B). There was also a

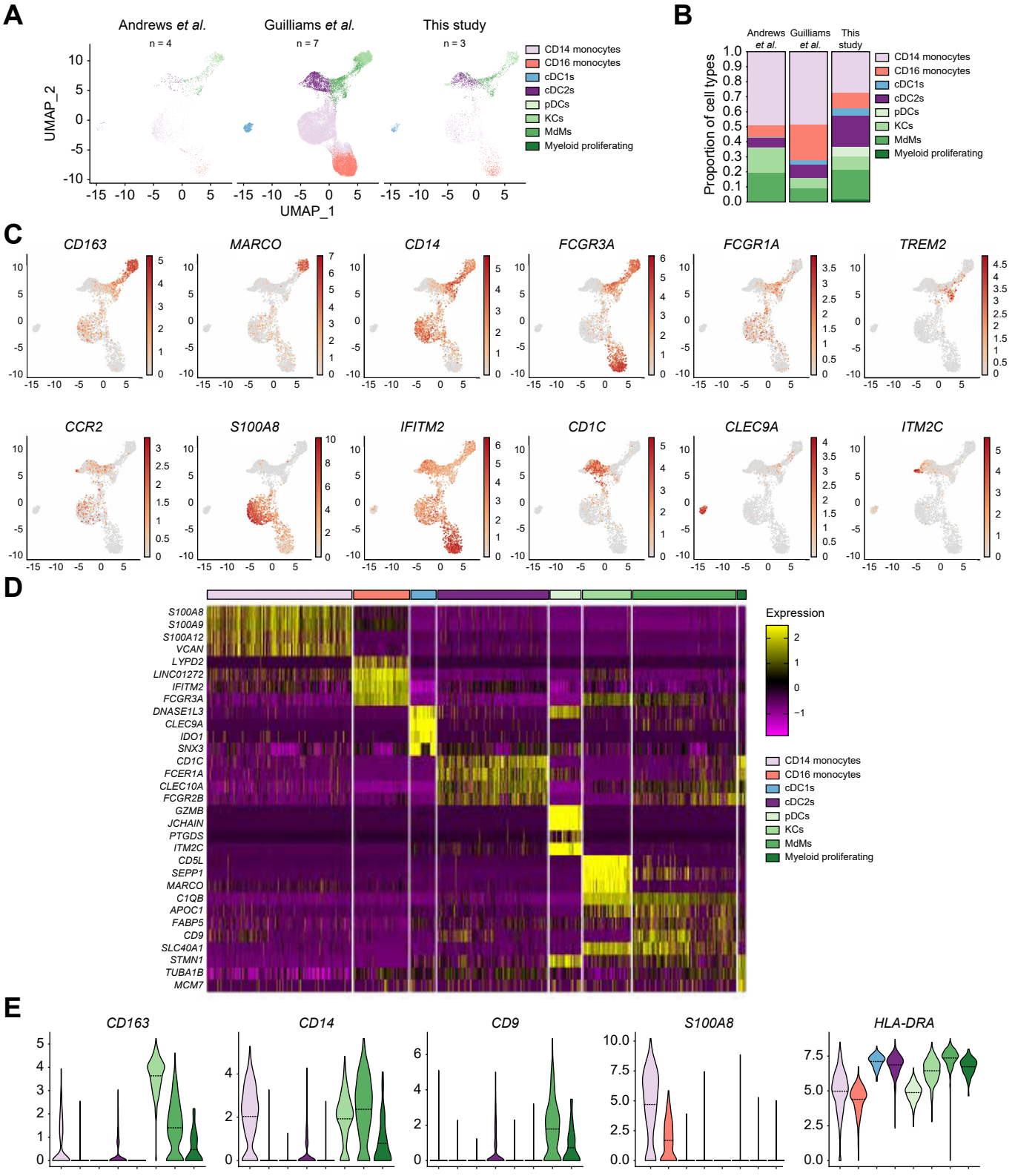

Fig. 3. ScRNA-seq analysis of myeloid cells from human livers. (A) UMAP plots of the eight myeloid cells clusters from the indicated scRNA-seq studies. (B) Myeloid cell composition from normal livers and the current study. (C) Expression scatter plots for the indicated genes across the eight clusters. (D) Heatmap of top four genes from each myeloid cell cluster indicated by the colour across the top. (E) Violin plots of selected genes across the eight myeloid clusters. cDC1, conventional DC 1; cDC2, conventional DC 2; DC, dendritic cell; KC, Kupffer cell; MdM, monocyte-derived macrophage; pDC, plasmacytoid DC; scRNA-seq, single-cell RNA sequencing; UMAP, uniform manifold approximation and projection.

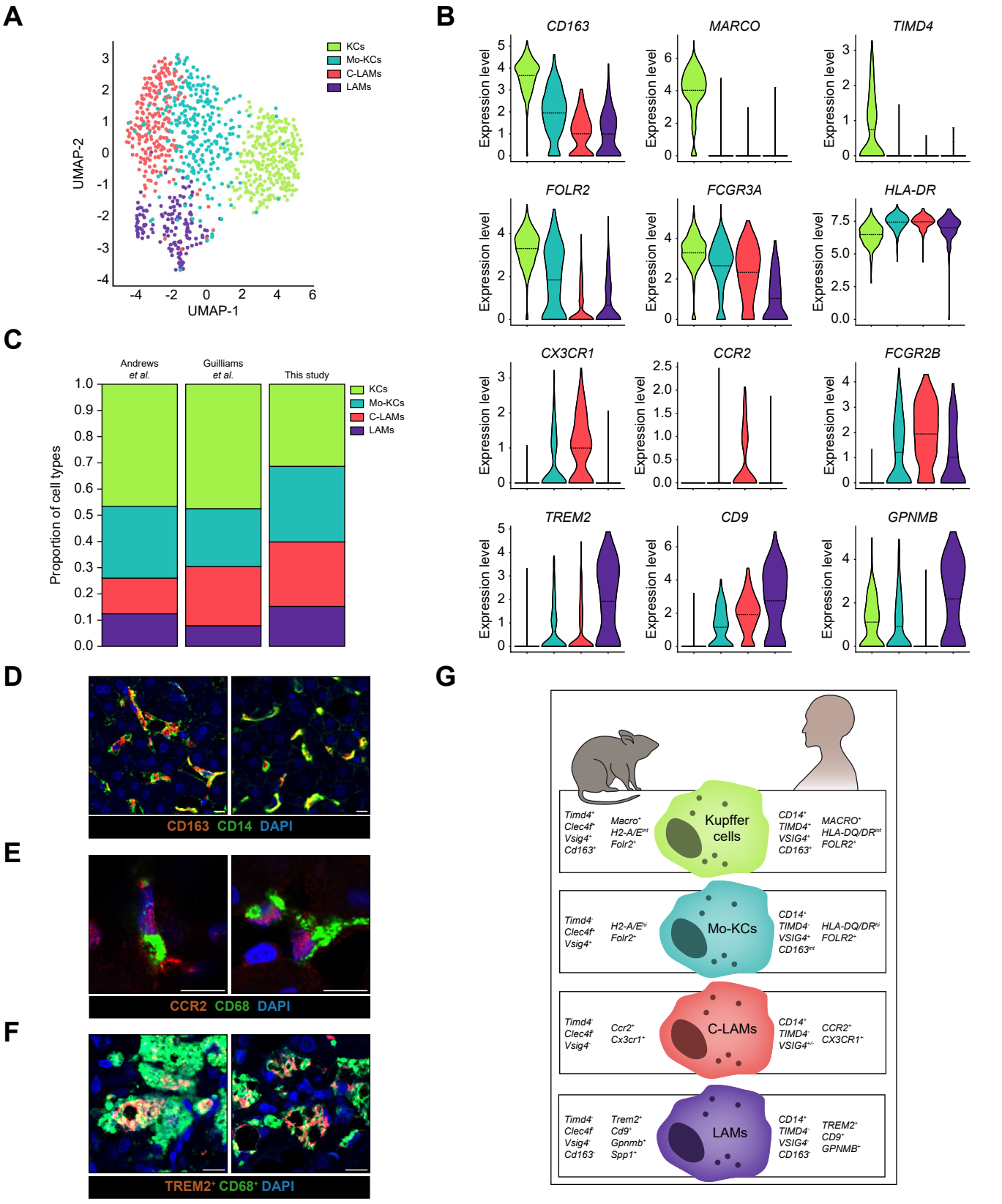

Fig. 4. Macrophage zoom reveals human macrophage subpopulations that align with those found in mice with MAFLD. (A) UMAP plot of four macrophage clusters in human MALFD liver. (B) Violin plots showing expression of select genes across the clusters of KCs, Mo-KCs, C-LAMs, and LAMs in the present dataset. (C) Comparison of macrophage subset distribution among published and present scRNA-seq datasets. (D) Representative immunofluorescence images of liver sections from two individuals showing CD163^{+} CD14^{+} human KCs. Red: CD163; green: CD14; blue: DAPI. Scale bar = 10 μm. (E) Representative immunofluorescence images of liver sections from two individuals showing CCR2^{+} CD68^{+} human C-LAMs. Red: CCR2; green: CD68; blue: DAPI. Scale bar = 10 μm. (F)

population of macrophages that expressed some KC markers (*FOLR2*, intermediate *CD163*) but lacked markers associated with mature, resident KC such as *MARCO* and *TIMD4* (Fig. 4B). These cells appear to be similar to the Mo-KCs that have been described in mouse models of NASH, and they align with markers for Mo-KCs published by Guilliams *et al.*[13] In general, there are few specific markers that define Mo-KCs as they overlap significantly with KCs (Table S5). Both KCs and Mo-KCs also had higher expression of *FCGR3A*, which encodes CD16 (Fig. 4B). Resident KCs had slightly lower expression of MHCII (*HLA-DR*) compared with MdMs in the human macrophage subsets, a profile that is observed in mouse models of MAFLD (Fig. 4B).[5] We also identified a subset of macrophages with higher expression of *TREM2*, *CD9*, and *GPNMB* (Fig. 4B). This gene expression profile aligns with that observed in hepatic LAMs identified in mouse models of NASH.[5,12] Analogous to the C-LAMs from mice, a population of *CX3CR1*/*CCR2*-expressing macrophages with lower-level expression of LAM genes was also identified (Fig. 4B).[5] We again integrated our data with that from the same two prior studies with healthy participants and noted that all clusters were represented in each sample set (Fig. 4C). When comparing our fatty liver samples with the healthier cohorts from Andrews *et al.*[18] and Guilliams *et al.*,[13] we found that the relative contribution of KCs was less (31 *vs*. 45 *vs*. 45%), whereas both Mo-KCs and C-LAMs/LAMs were slightly greater at 28 *vs*. 26 *vs*. 23%, and 40 *vs*. 26 *vs*. 30%, respectively (Fig. 4C).

To validate the scRNA-seq data, we performed immunofluorescence and confocal microscopy to assess macrophage populations in liver tissue. KCs were abundant and identified by co-expression of CD163 and CD14 in the tissues (Fig. 4D). Mo-KCs also express an intermediate level of CD163, making it difficult to specifically identify these macrophages. C-LAMs were identified as $CCR2^+$ $CD68^+$ macrophages, and LAMs were identified by colocalisation of TREM2 and CD68 (Fig. 4E and F). The majority of TREM2-positive macrophages were found in aggregates, similar to what has been observed for LAMs in mouse models of disease. Thus, macrophage subsets that align well with those found in mouse models of MAFLD can be found in the human liver (Fig. 4G).

Quantification of KCs and MdMs in the human liver via flow cytometry

To further assess macrophage and monocyte composition in human MAFLD, we also performed flow cytometry on liver samples. To minimise sampling bias for flow cytometry, we minced a large (~700 mg) piece of liver tissue and digested it in media containing collagenase. Non-parenchymal cells were partially purified by differential centrifugation. Single-cell suspensions were then prepared and stained with a panel of antibodies against CD45, CD14, CD16, CD163, HLA-DR, CD11b, CD64, and CCR2 (Fig. 5A). In the $CD14^+$ gate, KCs were identified by their high expression of CD163 and lower expression of CD64 (*FCGR1A*; Fig 5A). From the $CD163^{lo}$, $CD64^+$ population, we then gated on $CD16^+$ and $CCR2^+$, $MHCII^{hi}$ monocytes/macrophages (Fig. 3E). Using an alternate gating strategy, we also quantified total $CD14^+$ CCR2-expressing cells that include all monocytes/macrophages and demonstrated complete segregation of CD163-expressing cells from CCR2-expressing cells (Fig. 5A). The distribution of cell counts per gram of tissue for each of these subsets is shown in Fig. 5A. Of note, we did not have antibodies for TREM2 or GPNMB at the time of sample collection that worked for flow cytometry; however, based on our scRNA-seq data, most of these macrophages would be expected to reside in the $CD163^{lo}$, $MHCII^{hi}$ macrophage gate. Given that tissue characteristics can influence the efficiency of cell removal for flow cytometry analysis, we performed CD14 immunofluorescence staining on liver tissue from patients who were identified as having high or low numbers of $CD14^+$ cells via flow cytometry (Fig. 5B). The number of $CD14^+$ cells observed in liver tissue sections correlated well with flow data, suggesting that the tissue processing for flow cytometry did not dramatically influence the results (Fig. 5C).

Liver macrophage accumulation correlates with degree of steatosis

We next sought to investigate the relationship between macrophage composition and liver pathology. When we divided patients into low (≤5%), moderate (6–14%), and high (≥15%) levels of steatosis, we observed a statistically significant increase in $CD14^+$ cells and $CCR2^+$ cells in the high steatosis group compared with the low steatosis group (Fig. 6A). The $CD163^+$ KCs had a more variable relationship with steatosis. In addition, the $CCR2^+$ macrophages and $CD16^+$ macrophages showed a similar trend towards increased numbers with high steatosis but with a borderline p value (Fig. 6A). To gain further insight into the correlation between monocyte/macrophage number and steatosis, we performed logistic regression to compare cell number in liver tissue with percent steatosis by histology across all the samples. As seen in Fig. 6B, total $CD14^+$ cells and $CCR2^+$ cells correlated well with the degree of steatosis with r values of 0.86 and 0.77, respectively. In contrast, $CD163^+$ KC number had a weaker correlation with steatosis (r = 0.46, p =0.09). Similar results were seen when correlation analysis was performed between macrophage number and steatosis measured by MRI (Fig. S3A and B). Together, these findings demonstrate that the number of hepatic monocytes and MdMs correlates well with steatosis, whereas the resident macrophage population has a variable relationship. Interestingly, liver steatosis did not correlate with markers of systemic metabolic derangements such as $HgbA_{1c}$, insulin concentration, or fasting serum triglyceride level (Fig. S4A–C).

We also evaluated the relationship between NAS score and liver macrophage cell counts. The number of $CD14^+$ cells was increased in those with the highest NAS scores (p = 0.09); however, $CD163^+$ KCs showed a more variable distribution with a trend towards fewer numbers in the highest NAS group (Fig. 6C). Similar results were seen with the macrophage cell counts relative to lobular inflammation score (Fig. S5A and B). Furthermore, $CD14^+$ cell number did not track with the degree of fibrosis, whereas the number of $CD163^+$ KCs tended to be lower in the patients with a higher grade of fibrosis (Fig. 6D).

Representative immunofluorescence images of liver sections from two individuals showing $TREM2^+$ $CD68^+$ human LAMs. Red: TREM2; green: CD68; blue: DAPI. Scale bar = 10 μm. (G) Schematic diagram of key genes expressed in human and mouse liver macrophage subsets. C-LAM, *Ccr2*/*Cx3cr1*-expressing LAM; KC, Kupffer cell; LAM, lipid-associated macrophage; MAFLD, metabolic dysfunction-associated fatty liver disease; Mo-KC, monocyte-derived KC; scRNA-seq, single-cell RNA sequencing; UMAP, uniform manifold approximation and projection.

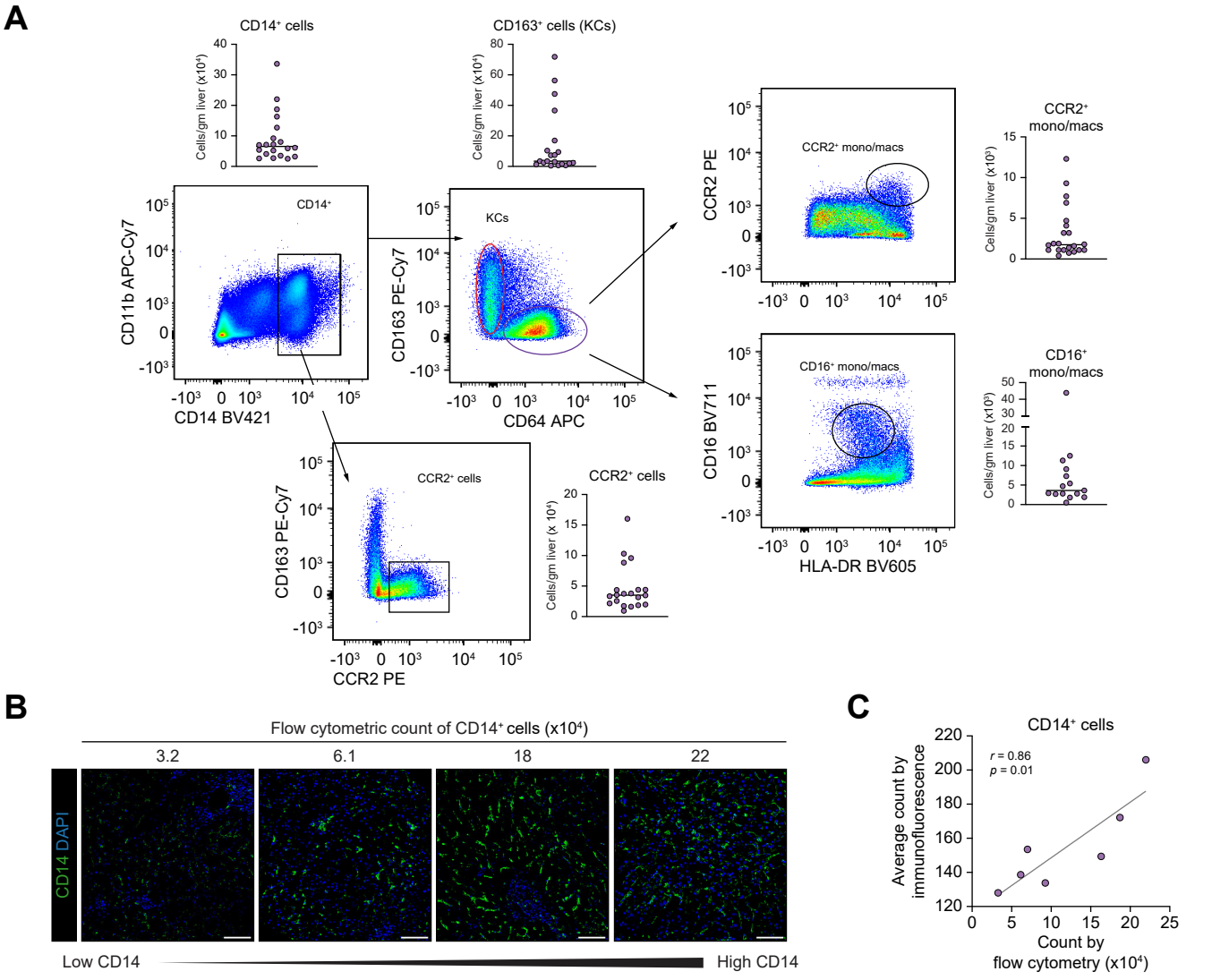

Fig. 5. Identification and quantification of human liver macrophage subsets by flow cytometry. (A) Gating strategy to identify different subsets of liver macrophages in human livers. The quantification of each population is shown by each representative flow plot. (B) Representative immunofluorescence staining of CD14 in human liver tissue of corresponding liver samples from patients with low and high numbers of $CD14^+$ cells by flow cytometry. (C) Correlation between average $CD14^+$ cells count per three to eight high-power fields in the liver tissue by immunofluorescence with count by flow cytometry. Value of *p* is shown (Pearson correlation coefficient). Green: CD14; blue: DAPI. Scale bar = 50 μm. KC, Kupffer cell.

MdM recruitment occurs with steatosis and precedes KC loss in pre-clinical models

Our human data revealed an expansion of total $CD14^+$ and $CCR2^+$ cells with steatosis in the absence of KC loss or liver injury. This is surprising in light of recent data from mouse models of NASH in which MdM accumulation is associated with a loss of resident KCs.[5,6] In fact, it has been proposed that the loss of KCs is an important signal for MdM influx.[7,20] Our observation implies either that MdM recruitment precedes KC loss in early fatty liver disease or that macrophage dynamics in MAFLD are fundamentally different across species. To explore these possibilities, mouse models designed to replicate earlier stages of MAFLD were used. To more closely approximate our human study participants, we used female mice, which tend to have milder metabolic phenotypes than males.[21] C57BL/6 female mice were fed short courses of either an HFSC diet (8-week duration) or a CDAA diet (2-week duration), and each was compared with control diet. The diets were initiated in a staggered fashion such that the mice were harvested and could be analysed at the same time to prevent batch effects (Fig. 7A). As expected, mice fed an HFSC diet had a slight gain in body weight and adipose tissue weight, whereas the CDAA diet-fed mice did not (Fig. 7B and Fig. S6A). However, the liver size increased in both diets (Fig. 7B and Fig. S6A). Hepatic monocyte/macrophage composition was assessed via flow cytometry and immunofluorescence imaging. By flow cytometry, liver macrophages were defined as $F4/80^{hi}$, $MHCII^{hi}$, and $Ly6C^{lo}$ cells (Fig. 7C). Resident KCs were identified by their expression of F4/80, CLEC2, VSIG4, and TIM4, whereas MdMs could be identified by lower expression of TIM4 (Fig. 7C).[5,6] The expression of VSIG4 allowed for further segregation of MdMs into Mo-KCs ($VSIG4^+$) and LAMs/C-LAMs ($VSIG4^-$; Fig. 7C).[10] A subset of immature C-LAMs does not express CLEC2, and these MdMs also increase modestly in the liver with CDAA diet (Fig. S6B). Total liver macrophage number and the number of resident KCs were similar across all groups, demonstrating that KC loss had not yet begun

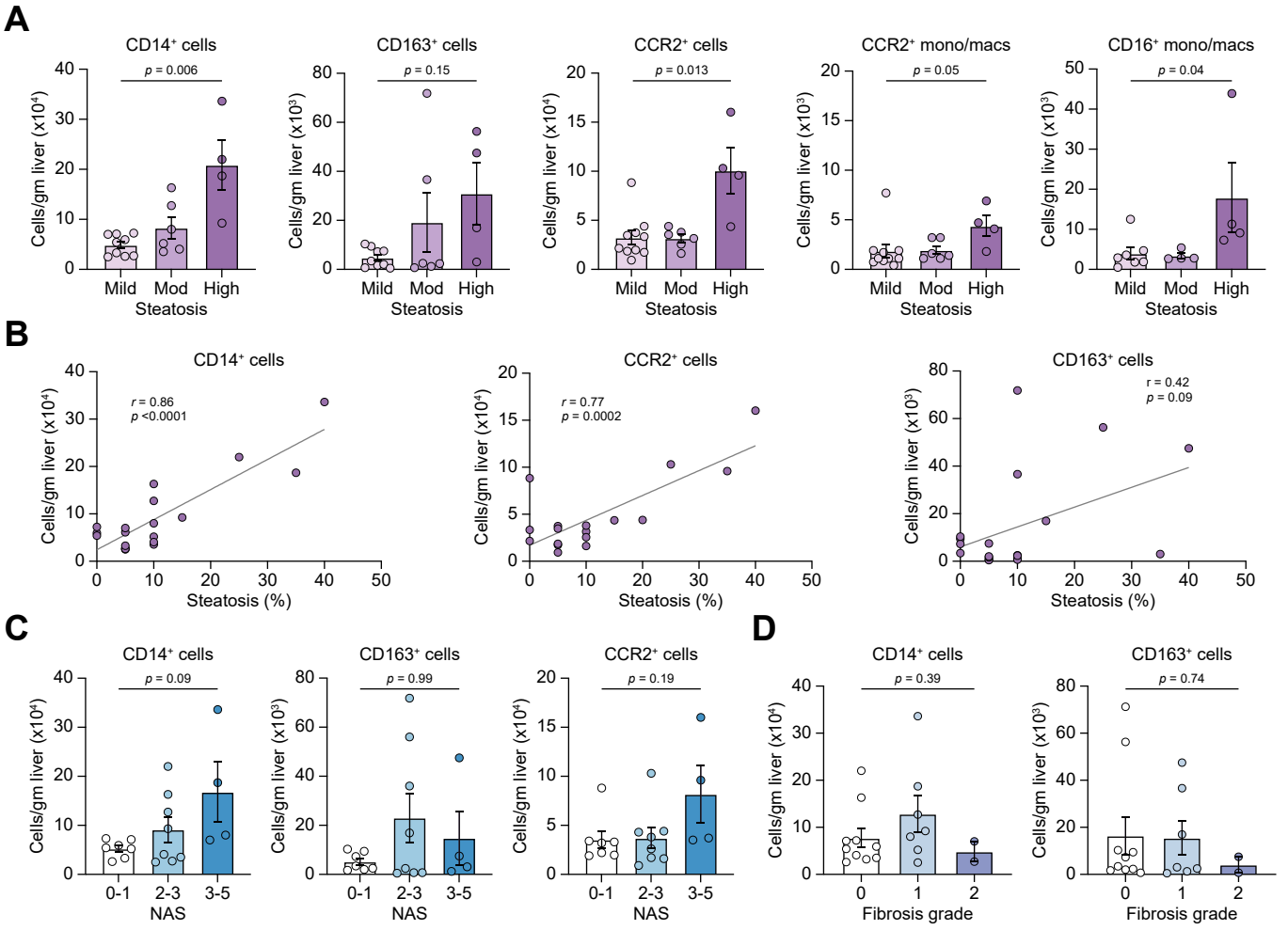

Fig. 6. Liver macrophage number directly correlates with steatosis in human during MAFLD. (A) Quantification of indicated macrophage populations (CD14, CD163, and CCR2) grouped by patient samples with mild (≤5%, n = 9), moderate (mod; 6–14%, n = 6) and high (≥15%, n = 4) levels of histological steatosis for which we had a total of 19 patients. (B) Correlation analysis of $CD14^+$, $CCR2^+$, or $CD163^+$ cells with histological steatosis. (C) Quantification of indicated cell populations grouped by patient samples with NAS scores of 0–1 (n = 7), 2–3 (n = 8), and 3–5 (n = 4). (D) Quantification of indicated cell populations grouped by patient samples with fibrosis grades of 0 (n = 10), 1 (n = 7), and 2 (n = 2). Values of *p* are shown; (A, C, and D) Kruskal–Wallis test and (B) Pearson correlational coefficient. MAFLD, metabolic dysfunction-associated fatty liver disease; NAFLD, non-alcoholic fatty liver disease; NAS, NAFLD activity score.

(Fig. 7D and E and Fig. S6C). However, there was a significant increase in liver MdMs (Mo-KCs and LAMs/C-LAMs) with both diets compared with STD (Fig. 7F and G and Fig. S6C). Mice fed the CDAA diet also had elevated numbers of total $CD45^+$ cells, $Ly6C^{hi}$ monocytes, immature MdMs ($F4/80^{hi}$, $CLEC2^-$; Fig. S6B), and cDC2 (Fig. S6D). These findings were true whether cell number was assessed per gram of liver tissue (Fig. 7D and G) or per liver (Fig. S6B–D).

To evaluate steatosis, we stained frozen sections of liver tissue with antibodies for perilipin-2 to highlight neutral lipid droplets. Low-power images demonstrated a substantial increase in steatosis with both the HFSC diet- and CDAA diet-fed mice compared with STD-fed mice (Fig. 7H). $F4/80^+$ macrophages were abundant throughout the liver regardless of the diet (Fig. 7H). However, macrophages in the steatotic liver often formed aggregates, a pattern that is distinct from the healthy liver and reminiscent of the formation of a hepatic crown-like structure (Fig. 7H and J). Consistent with the preservation of resident KCs via the flow cytometric data, $TIM4^+$-resident KCs could be found throughout the liver irrespective of diet (Fig. 7I). However, MdMs ($CD68^+$ $TIM4^-$) were only observed in the livers of mice fed the HFSC or CDAA diets (Fig. 7J).

MdMs take up lipids from lipid-loaded hepatocytes

The observation that MdMs are recruited to the liver during the early stages of steatosis in human and mice suggested that they may have a role in interacting with lipids. To gain insight into this possibility *in vivo*, we flow-sorted MdMs and KCs from mice fed an HFHS diet for 4 months and performed transmission electron microscopy (Fig. 8A). This time point was chosen to allow for the expansion of the MdM populations enough to facilitate imaging via electron microscopy. We noted that the LAMs/C-LAMs are smaller than KCs and Mo-KCs (Fig. S7A). Intriguingly, MdMs including Mo-KCs and LAMs/C-LAMs had more lipid droplets with significantly greater lipid droplet area than the resident KCs (Fig. 8B–E and Fig. S7B). Thus, MdMs

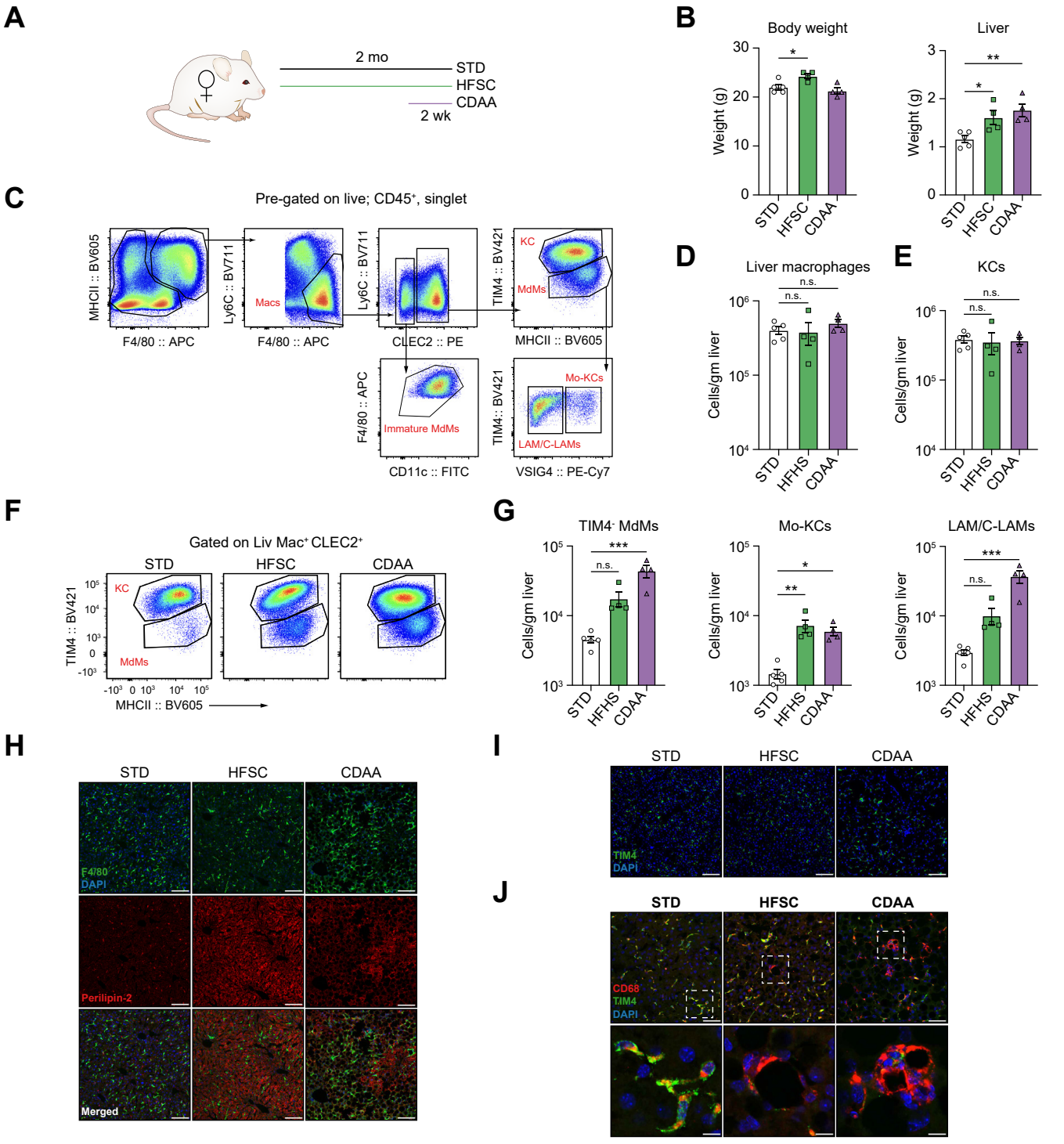

Fig. 7. Mouse models of early MAFLD recapitulate MdM expansion with steatosis. (A) Schematic of diet experiments in C57BL/6 mice. (B) Final body and liver weights of animals. (C) Gating strategy for identifying macrophage subsets in the liver. (D) Quantification of liver macrophages (as defined by the gating strategy depicted in C) per gram of liver tissue by flow cytometry. (E) Quantification of KCs per gram of liver tissue by flow cytometry. (F) Representative flow cytometry plots showing the expansion of TIM4$^-$ MdMs in HFSC and CDAA diets. (G) Quantification of MdMs, Mo-KCs, and LAM/C-LAMs per gram of liver tissue by flow cytometry. (H) Representative immunofluorescence images of F4/80$^+$ macrophages and perilipin-2 in the livers isolated from animals fed different diets. Green: F4/80; red: perilipin-2; blue: DAPI. Scale bar = 100 μm. (I) Representative immunofluorescence images of TIM4$^+$ KCs in the livers isolated from animals fed different diets. Green: TIM4; blue: DAPI. Scalebar = 100 μm. (J) CD68$^+$ TIM4$^+$ KCs and CD68$^+$ TIM4$^-$ MdMs in the livers isolated from animals fed different diets. Red: CD68; green: TIM4; blue: DAPI. Scale bar = 50 μm for low-power images and 10 μm for zoomed-in inserts. Coloured bars represent the mean ± SEM. Each dot represents an individual mouse. *p <0.05, **p <0.01, ***p <0.001 (one-way ANOVA). C-LAM, *Ccr2*/*Cx3cr1*-expressing LAM; CDAA, choline-deficient amino acid; HFSC, high-fat, high-sucrose, and high-cholesterol; KC, Kupffer cell; LAM, lipid-associated macrophage; MAFLD, metabolic dysfunction-associated fatty liver disease; MdM, monocyte-derived macrophage; MHC, major histocompatibility complex; MHCII, MHC class II; Mo-KC, monocyte-derived macrophage; STD, standard chow diet.

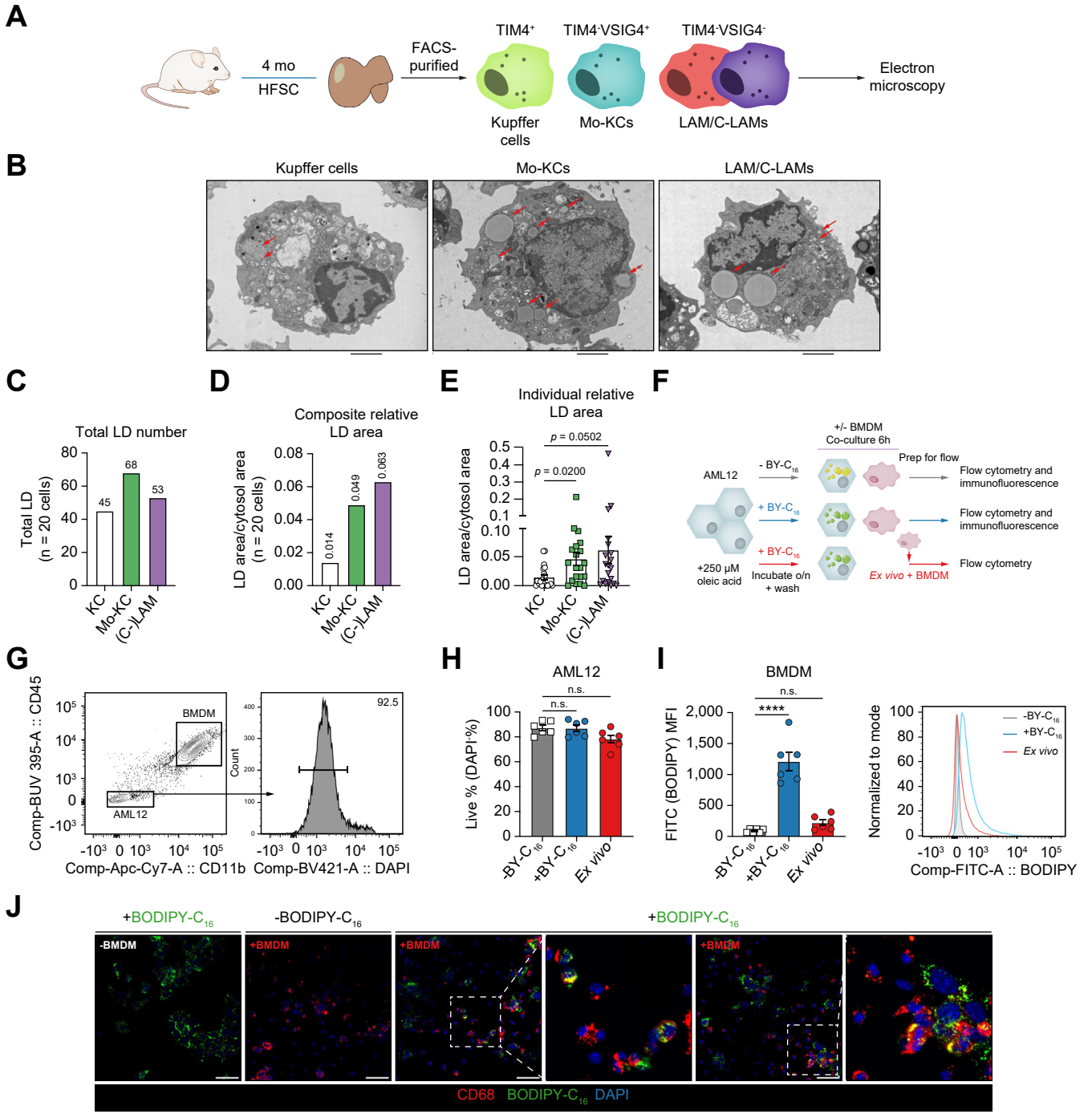

Fig. 8. Monocyte-derived macrophages accumulate lipid in MAFLD. (A) Schematic of diet experiment in C57BL/6 mice and cell sorting for electron microscopy. (B) Representative electron micrographs of KC, Mo-KC, and LAM/C-LAM. LDs are indicated by red arrows. Scale bar = 2 µm. (C) Quantification of the total number of LDs in 20 cells per cell type. (D) Quantification of the composite relative LD area as calculated by total LD area divided by total cytosol area of 20 cells per cell type. (E) Quantification of individual relative LD area as calculated by total LD area per cell divided by total cytosol area per cell. (F) Schematic of coculture experiments of lipid-laden hepatocytes (AML12) with BMDMs. (G) Representative flow plot identifying BMDM and AML12 cells and live cells within the AML12 population. (H) Percentage of live ($DAPI^-$) AML12 cells from coculture experiments described in (F). (I) Quantification of BODIPY signal as MFI in BMDMs from coculture experiments described in (F). A representative flow plot is also shown. (J) Representative immunofluorescence images of monoculture or coculture of AML12 with BMDMs as described in (F). Zoom-in images highlight the colocalisation of green lipids with red macrophages. Red: CD68; green: BY-C_{16}; blue: DAPI. Scalebar = 50 µm. Bars represent the mean ± SEM. Each dot represents an individual cell (E) or well of cells (H and I). *p <0.05, **p <0.01, ***p <0.001, ****p <0.0001; (E) Kruskal–Wallis test and (H and I) one-way ANOVA. BMDM, bone marrow-derived macrophage; BY-C_{16}, BODIPY-C_{16}; C-LAM, *Ccr2*/*Cx3cr1*-expressing LAM; FITC, fluorescein isothiocyanate; HFSC, high-fat, high-sucrose, and high-cholesterol; KC, Kupffer cell; LAM, lipid-associated macrophage; LD, liquid droplet; MAFLD, metabolic dysfunction-associated fatty liver disease; MFI, mean fluorescence intensity; Mo-KC, monocyte-derived macrophage.

appeared to accumulate more lipid than resident KCs do during MAFLD.

Based on this finding, we conducted coculture experiments to address whether MdMs take up hepatocyte-derived lipids (Fig. 8F). For these experiments, we incubated AML12 cells, a mouse hepatocyte cell line, with oleate combined with a low concentration of BODIPY-C_{16} (BY–C_{16}) overnight to generate hepatocytes with fluorescent-labeled lipid droplets. After washing the cells to remove any free BY-C_{16}, we mixed bone marrow-derived macrophages (BMDMs) with these lipid-laden hepatocytes and cocultured them together for 6 h. Importantly, oleate incubation did not cause toxicity to hepatocytes (Fig. 8G and H). After the incubation period, BODIPY signal was readily detected in the lipid droplets within the hepatocytes (Fig. 8J, first panel). To quantify lipid transfer by flow cytometry, BODIPY signal was assessed in $CD45^+$ $CD11b^+$ macrophages. BODIPY fluorescence could be detected in macrophages only when they were co-incubated with hepatocytes containing BY-C_{16} (Fig. 8I). As an additional control, we also mixed BY-C_{16}-labelled hepatocytes with macrophages at the time of cell harvest to ensure that transfer did not occur during the processing of the cells for flow analysis (*ex vivo* control) (Fig. 8F and I). To further validate these findings, we performed confocal microscopy, which revealed BODIPY signal in the $CD68^+$ macrophages (Fig. 8J). Together, these findings demonstrate that MdMs are capable of taking up fat released from lipid-laden hepatocytes.

Discussion

Macrophages are important contributors to the pathogenesis of fatty liver disease and NASH. In this study, we used human liver samples from morbidly obese patients undergoing bariatric surgery to gain insight into the inflammatory phenotype of early MAFLD in humans. Using scRNA-seq, flow cytometry, tissue imaging, and clinical data, we made several observations. First, our study demonstrated that the steatotic human liver contains macrophage subsets with gene expression signatures similar to those described in mouse models of MAFLD. Second, we found that the number of $CD14^+$ cells in the liver correlated well with the degree of steatosis, whereas this was not true for CD163, a marker of resident KCs. Third, using two diet models of early liver steatosis in mice, we showed that recruitment of MdMs precedes tissue damage and loss of KCs. Lastly, we provide evidence that MdMs preferentially take up lipids from steatotic hepatocytes. Together, these findings provide insight into human macrophage heterogeneity in MAFLD and demonstrate parallels with preclinical models of disease. Moreover, mouse model data prompted by our human studies demonstrated that early recruitment of MdMs to liver is associated with steatosis independent of KC death or tissue damage, and these MdMs might perform unique lipid handling functions.

Our understanding of macrophage diversity in murine MAFLD has exploded with several recent studies combining fate-mapping and scRNA-seq approaches.[5–8,19,22] Whether similar populations of macrophages exist in humans with MAFLD has been a subject of debate. In one recent study that used spatial transcriptomics, a small subset of macrophages that resembled LAMs was observed in the healthy human livers, and these macrophages became proportionally greater in number with a different tissue distribution in the steatotic livers.[13] However, only four liver samples from this study contained >10% steatosis. In contrast, another recent study used both scRNA-seq and whole liver tissue bulk RNA sequencing from humans with various stages of MAFLD and suggested that macrophages with a LAM phenotype were rare in humans.[15] Rather, they describe a population of calgranulin (*S100A8*/*A9*) expressing 'macrophages' that correlated with fibrosis. Thus, the conservation of macrophage subtypes in MAFLD across species remains controversial.

In our study, scRNA-seq of myeloid cells identified monocytes, dendritic cells, and macrophages. Of the two monocyte clusters, the $CD14^{hi}$ subset had overlapping gene expression with the *S100A8*-expressing cells described in the study by Fred *et al.*,[15] which included *MNDA*, *VCAN*, *CTSA*, and *LYZ*, arguing that these cells are monocytes. To further delineate macrophage signatures in the human liver, we zoomed in on these cells in our scRNA-seq data and were able to resolve four distinct subsets. Interestingly, the gene expression features of our macrophage clusters resembled that seen for KCs, Mo-KCs, LAMs, and C-LAMs reported in the murine NASH liver. Using immunofluorescence imaging, we were also able to provide evidence that these macrophage subsets could be observed in the human liver. Of these macrophages, KCs and Mo-KCs accounted for ~60%, with the remaining 40% being C-LAMs/LAMs. This is in contrast to the report from Fred *et al.*,[15] which concluded that LAMs were a rare population via bulk or scRNA-seq. Although the reason for this discrepancy is not clear, it may be related to the fact that smaller pieces of liver were used (100 *vs.* 500–1,000 mg) and the scRNA-seq was not pregated on $CD45^+$ cells, as was done in our study. Together, our findings with those from the study by Guillams *et al.*[13] support the conclusion that the human MAFLD liver contains several distinct subtypes of macrophages, which align well with mouse data from models of fatty liver disease. To gain additional insight, we also integrated our dataset with scRNA-seq data from two recent studies that included relatively normal 'healthy controls'.[13,18] This comparison demonstrated that all the myeloid clusters were present in both controls and the steatotic livers. However, among the macrophages, there was a slight enrichment of C-LAMs/LAMs and a relative decrease in KCs from our steatotic samples. This observation suggests good alignment between macrophages in the steatotic murine and human liver, which has implications for the use of preclinical models to evaluate the translation of immunomodulatory therapies to humans.

The majority of human tissue that has been available for studies of MAFLD and NASH is frequently obtained from patients in whom liver biopsy is performed for clinical reasons. Therefore, these samples tend to represent later stages of the disease. Our patient cohort consisted of females with morbid obesity and earlier stages of MAFLD from whom we could obtain a significant amount of tissue at the time of bariatric surgery. This allowed us to conduct flow cytometry in conjunction with tissue imaging and scRNA-seq. In addition, we used MRI data to quantify total liver steatosis. Although there was significant variability in the degree of liver steatosis between patients, there was a strong correlation between MRI and histologic assessment of liver fat, which enhances the conclusions that can be drawn from our data. We found that the number of total macrophage/monocyte ($CD14^+$) and other MdM subgroups correlated with the degree of tissue steatosis. In contrast, CD163-expressing KCs had a more variable relationship with the degree of steatosis. Although CD163 is a very good marker for KCs, VSIG4 and FOLR2 have recently been proposed as optimal markers for the identification of human KCs.[13] Our analysis had already been conducted before these results were published and therefore were unable to add these markers to our antibody panel. We also compared hepatic myeloid cell number across the spectrum of

NASH activity (as assessed by NAS score). Only two samples qualified for a diagnosis of NASH (NAS ≥5). However, we found that $CD14^+$ cells were increased in the patients with the highest NAS score, whereas the KC number tended to be lower in this subset. The degree of liver fibrosis was mild in our cohort, which limited our ability to observe patterns between macrophage subtype and fibrosis grade. However, prior studies of more advanced liver disease have consistently shown an increased number of CCR2-expressing macrophages that associate with fibrosis and appear to play a role in matrix deposition and remodelling.[14,23] In summary, we provide evidence that in early MAFLD in humans, there is a tight association between liver steatosis and recruitment of monocytes and MdMs.

The observation that MdMs accumulated in the human liver before evidence of damage (normal alanine aminotransferase and minimal fibrosis) or KC loss in steatotic livers was unexpected based on findings with preclinical models of disease. In fact, prior mouse studies have suggested that KC loss is an important trigger for MdM recruitment in both chemically induced depletion studies[24,25] and in NASH.[7,20] Our human results argued either that early MdM recruitment with liver steatosis occurs independent of KC loss/tissue damage or that mouse and human models of the disease have distinct macrophage dynamics. To distinguish these possibilities, we fed female mice two distinct diets to induce early liver steatosis and also observed that MdMs entered the mouse liver before KC depletion. Thus, similar to what was observed in human samples, the initial MdM recruitment begins with steatosis and precedes KC loss or fibrosis. This observation highlights the time-dependent phases of macrophage compositional changes that happen during MAFLD and cautions against overinterpreting snapshot time points. Although it remains to be determined whether KC loss happens in humans with more advanced NASH, there does appear to be loss of at least a subset of KCs in the cirrhotic human liver.[14]

Although the functions of MdMs in MAFLD are heterogenous, we provide evidence that infiltrating macrophages accumulate more lipid droplets than resident KCs in a mouse model of MAFLD. Moreover, using a coculture system, we demonstrate that bone marrow monocyte-derived cells are capable of taking up lipids originating from fatty acid-loaded hepatocytes. These findings are intriguing in light of recent data indicating that steatotic hepatocytes release extracellular vesicles that contain fatty acids.[26] Although it has been suggested that these extracellular vesicles can be proinflammatory, further work will be necessary to understand the consequences of lipid transplant and the fate of the ingested fatty acids. Together, these observations suggest that infiltrating macrophages readily ingest lipids and raise the possibility that they may have a role in lipid handling during liver steatosis.

Limitations

There are several limitations to the current study that must be acknowledged. The scRNA-seq could only be performed on three patients, all of whom had liver steatosis, and therefore, there is not a true normal liver group for comparison of macrophage subpopulations. To partially overcome this limitation, we integrated our data with two other scRNA-seq datasets containing control liver samples; however, we acknowledge that there can be differences in sample collection, processing, and analysis that confound some of these comparisons. For the flow cytometry assessment of liver tissue, there were markers identified via scRNA-seq that could not be probed owing to a lack of reliable staining antibodies at the time the experiments were conducted. In addition, the quantification of immune cells by flow cytometry can be influenced by extraction efficiency. However, we used immunofluorescence as a strategy to validate the trends seen by flow cytometry. In the murine study, we defined LAM/C-LAMs as $TIM4^-VSIG4^-$ macrophage. Nevertheless, this double-negative population may also include progenitors of Mo-KCs that have yet to upregulate Mo-KC-specific markers (*e.g.* VSIG4 and CLEC4F). Lastly, our patient population was a female cohort with obesity, and therefore, it is not clear how these results would apply to males with MAFLD.

Conclusions

In this study, we present data on liver macrophage populations from 21 female participants with obesity and with variable degrees of liver steatosis and no significant fibrosis. Using transcriptional analysis, tissue imaging, and flow cytometry, we provide evidence that macrophage subpopulations in MAFLD are well aligned between mice and humans. Moreover, MdM entry to the liver correlates with steatosis and, at earlier stages of MAFLD, is not driven by KC loss. Compared with KCs, MdMs also appear to take up more lipids in the fatty liver, suggesting that they may contribute to lipid handling in disease. Given the role of macrophages in tissue remodelling during NASH, defining the relationship of macrophage identity between humans and mice with MAFLD is of critical translational importance.

Abbreviations

BMDM, bone marrow-derived macrophage; BY-C_{16}, BODIPY-C_{16}; C-LAM, *Ccr2*/*Cx3cr1*-expressing LAM; CDAA, choline-deficient amino acid; cDC1, conventional DC 1; cDC2, conventional DC 2; DC, dendritic cell; HFSC, high-fat; high-sucrose, and high-cholesterol; $HgbA_{1c}$, haemoglobin A_{1c}; KC, Kupffer cell; LAM, lipid-associated macrophage; MAFLD, metabolic dysfunction-associated fatty liver disease; MdM, monocyte-derived macrophage; MHCII, MHC class II; Mo-KC, monocyte-derived KC; MRI, magnetic resonance imaging; NAFLD, non-alcoholic fatty liver disease; NAS, NAFLD activity score; pDC, plasmacytoid DC; scRNA-seq, single-cell RNA sequencing; STD, standard chow diet; UMAP, uniform manifold approximation and projection.

Financial support

This work was supported by NIH grants R01 DK11003401 (JDS), R01 DK13118801 (JDS and BR), and R01 DK104735 (BNF); ADA 118-IBS280 (JDS); NSF DGE-1745038/DGE-2139839 (MMC); and the Pershing Square Foundation (SK). The core services of the Diabetes Research Center (P30 DK020579) and the Nutrition Obesity Research Center (P30 DK56341) at Washington University School of Medicine also supported this work.

Conflicts of interest

BF is a member of the Scientific Advisory Board and owns stock in Cirius Therapeutics, which is developing an MPC inhibitor for clinical use in treating NASH.

Please refer to the accompanying ICMJE disclosure forms for further details.

Authors' contributions

Conceptualisation: JS, SK, JB. Methodology – visualisation: JS, SK, SD, MA, JB, WB, AP. Software formal analysis: MA, MT. Investigation: MMC, SD, LH, MT, BY, JB, GS, KB, SE, JE, DF, BF. Data curation: JS, SD, MMC. Writing –

original draft preparation: JS, MMC. Writing – review and editing: JS, MMC, SK, BR, JB, GS. Supervision and project administration: JS, SK, JB, GS. Funding acquisition: JS, SK. Have read and agreed to the published version of the manuscript: all authors.

Data availability statement

All data are available upon request from the corresponding author.

Supplementary data

Supplementary data to this article can be found online at https://doi.org/10.1016/j.jhepr.2023.100877.

References

Author names in bold designate shared co-first authorship.

[1] Kaya E, Yilmaz Y. Metabolic-associated fatty liver disease (MAFLD): a multisystemic disease beyond the liver. J Clin Transl Hepatol 2022;10:329–338.

[2] Ferguson D, Finck BN. Emerging therapeutic approaches for the treatment of NAFLD and type 2 diabetes mellitus. Nat Rev Endocrinol 2021;17:484–495.

[3] Wree A, Broderick L, Canbay A, Hoffman HM, Feldstein AE. From NAFLD to NASH to cirrhosis – new insights into disease mechanisms. Nat Rev Gastroenterol Hepatol 2013;10:627–636.

[4] Younossi Z, Anstee QM, Marietti M, Hardy T, Henry L, Eslam M, et al. Global burden of NAFLD and NASH: trends, predictions, risk factors and prevention. Nat Rev Gastroenterol Hepatol 2018;15:11–20.

[5] Daemen S, Gainullina A, Kalugotla G, He L, Chan MM, Beals JW, et al. Dynamic shifts in the composition of resident and recruited macrophages influence tissue remodeling in NASH. Cell Rep 2021;34:108626.

[6] Remmerie A, Martens L, Thoné T, Castoldi A, Seurinck R, Pavie B, et al. Osteopontin expression identifies a subset of recruited macrophages distinct from Kupffer cells in the fatty liver. Immunity 2020;53:641–657.e614.

[7] Tran S, Baba I, Poupel L, Dussaud S, Moreau M, Gelineau A, et al. Impaired Kupffer cell self-renewal alters the liver response to lipid overload during non-alcoholic Steatohepatitis. Immunity 2020;53:627–640.e5.

[8] Seidman JS, Troutman TD, Sakai M, Gola A, Spann NJ, Bennett H, et al. Niche-specific reprogramming of epigenetic landscapes drives myeloid cell diversity in nonalcoholic steatohepatitis. Immunity 2020;52:1057–1074.e1057.

[9] Jaitin DA, Adlung L, Thaiss CA, Weiner A, Li B, Descamps H, et al. Lipid-associated macrophages control metabolic homeostasis in a Trem2-dependent manner. Cell 2019;178:686–698.e614.

[10] Daemen S, Chan MM, Schilling JD. Comprehensive analysis of liver macrophage composition by flow cytometry and immunofluorescence in murine NASH. STAR Protoc 2021;2:100511.

[11] **Calcagno DM**, **Chu A**, Gaul S, Taghdiri N, Toomu A, Leszczynska A, et al. NOD-like receptor protein 3 activation causes spontaneous inflammation and fibrosis that mimics human NASH. Hepatology 2022;76:727–741.

[12] Remmerie A, Martens L, Scott CL. Macrophage subsets in obesity, aligning the liver and adipose tissue. Front Endocrinol 2020;11:259.

[13] Guilliams M, Bonnardel J, Haest B, Vanderborght B, Wagner C, Remmerie A, et al. Spatial proteogenomics reveals distinct and evolutionarily conserved hepatic macrophage niches. Cell 2022;185:379–396.e338.

[14] Ramachandran P, Dobie R, Wilson-Kanamori JR, Dora EF, Henderson BEP, Luu NT, et al. Resolving the fibrotic niche of human liver cirrhosis at single-cell level. Nature 2019;575:512–518.

[15] Fred RG, Steen Pedersen J, Thompson JJ, Lee J, Timshel PN, Stender S, et al. Single-cell transcriptome and cell type-specific molecular pathways of human non-alcoholic steatohepatitis. Sci Rep 2022;12:13484.

[16] MacParland SA, Liu JC, Ma XZ, Innes BT, Bartczak AM, Gage BK, et al. Single cell RNA sequencing of human liver reveals distinct intrahepatic macrophage populations. Nat Commun 2018;9:4383.

[17] Brunt EM, Kleiner DE, Wilson LA, Belt P, Neuschwander-Tetri BA, NASH Clinical Research Network (CRN). Nonalcoholic fatty liver disease (NAFLD) activity score and the histopathologic diagnosis in NAFLD: distinct clinicopathologic meanings. Hepatology 2011;53:810–820.

[18] Andrews TS, Atif J, Liu JC, Perciani CT, Ma XZ, Thoeni C, et al. Single-cell, single-nucleus, and spatial RNA sequencing of the human liver identifies cholangiocyte and mesenchymal heterogeneity. Hepatol Commun 2022;6:821–840.

[19] Guilliams M, Scott CL. Liver macrophages in health and disease. Immunity 2022;55:1515–1529.

[20] Devisscher L, Scott CL, Lefere S, Raevens S, Bogaerts E, Paridaens A, et al. Non-alcoholic steatohepatitis induces transient changes within the liver macrophage pool. Cell Immunol 2017;322:74–83.

[21] Strack C, Behrens G, Sag S, Mohr M, Zeller J, Lahmann C, et al. Gender differences in cardiometabolic health and disease in a cross-sectional observational obesity study. Biol Sex Differ 2022;13:8.

[22] **Barreby E**, **Chen P**, **Aouadi M**. Macrophage functional diversity in NAFLD – more than inflammation. Nat Rev Endocrinol 2022;18:461–472.

[23] Krenkel O, Puengel T, Govaere O, Abdallah AT, Mossanen JC, Kohlhepp M, et al. Therapeutic inhibition of inflammatory monocyte recruitment reduces steatohepatitis and liver fibrosis. Hepatology 2018;67:1270–1283.

[24] Scott CL, Zheng F, De Baetselier P, Martens L, Saeys Y, De Prijck S, et al. Bone marrow-derived monocytes give rise to self-renewing and fully differentiated Kupffer cells. Nat Commun 2016;7:10321.

[25] Bonnardel J, T'Jonck W, Gaublomme D, Browaeys R, Scott CL, Martens L, et al. Stellate cells, hepatocytes, and endothelial cells imprint the Kupffer cell identity on monocytes colonizing the liver macrophage niche. Immunity 2019;51:638–654.e639.

[26] **Garcia-Martinez I**, **Alen R**, Pereira L, Povo-Retana A, Astudillo AM, Hitos AB, et al. Saturated fatty acid-enriched small extracellular vesicles mediate a crosstalk inducing liver inflammation and hepatocyte insulin resistance. JHEP Rep 2023;5:100756.